Received: 16 October 2020 | Revised: 9 December 2020 | Accepted: 9 December 2020

DOI: 10.1002/mrm.28664

FULL PAPER

Magnetic Resonance in Medicine

Iron(III)-*t*CDTA derivatives as MRI contrast agents: Increased T_1 relaxivities at higher magnetic field strength and pH sensing

Jing Xie[1] | **Akvile Haeckel**[1] | **Ralf Hauptmann**[1] | **Iweta Pryjomska Ray**[2] | **Christian Limberg**[2] | **Nora Kulak**[3] | **Bernd Hamm**[1] | **Eyk Schellenberger**[1]

[1]Department of Radiology, Charité–Universitätsmedizin Berlin, Berlin, Germany

[2]Department of Chemistry, Humboldt-Universität zu Berlin, Berlin, Germany

[3]Institute of Chemistry, Otto-von-Guericke-Universität Magdeburg, Magdeburg, Germany

Correspondence
Eyk Schellenberger, Department of Radiology, Charité–Universitätsmedizin Berlin, Charitéplatz 1, 10117 Berlin, Germany.
Email: eyk.schellenberger@charite.de

Funding Information
Supported by the Deutsche Forschungsgemeinschaft (DFG, SCHE 1416/11-1 and sub-project B08 of the SFB-1340)

Purpose: Low molecular weight iron(III) complex-based contrast agents (IBCA) including iron(III) *trans*-cyclohexane diamine tetraacetic acid $[Fe(t\text{CDTA})]^-$ could serve as alternatives to gadolinium-based contrast agents in MRI. In search for IBCA with enhanced properties, we synthesized derivatives of $[Fe(t\text{CDTA})]^-$ and compared their contrast effects.

Methods: *Trans*-cyclohexane diamine tetraacetic acid (*t*CDTA) was chemically modified in 2 steps: first the monoanhydride of *Trans*-cyclohexane diamine tetraacetic acid was generated, and then it was coupled to amines in the second step. After purification, the chelators were analyzed by high-performance liquid chromatography, mass spectrometry, and NMR spectrometry. The chelators were complexed with iron(III), and the relaxivities of the complexes were measured at 0.94, 1.5, 3, and 7 Tesla. Kinetic stabilities of the complexes were analyzed spectrophotometrically and the redox properties by cyclic voltammetry.

Results: Using ethylenediamine (en) and *trans*-1,4-diaminocyclohexane, we generated monomers and dimers of *t*CDTA: en-*t*CDTA, en-*t*CDTA-dimer, *trans*-1,4-diaminocyclohexane-*t*CDTA, and *trans*-1,4-diaminocyclohexane-*t*CDTA-dimer. The iron(III) complexes of these derivatives had similarly high stabilities as $[Fe(t\text{CDTA})]^-$. The iron(III) complexes of the *trans*-1,4-diaminocyclohexane derivatives had higher T_1 relaxivities than $[Fe(t\text{CDTA})]^-$ that increased with increasing magnetic field strengths and were highest at 6.8 $L{\cdot}mmol^{-1}{\cdot}s^{-1}$ per molecule for the dimer. Remarkably, the relaxivity of $[Fe(\text{en-}t\text{CDTA})]^+$ had a threefold increase from neutral pH toward pH6.

Conclusion: Four iron(III) complexes with similar stability in comparison to $[Fe(t\text{CDTA})]^-$ were synthesized. The relaxivities of *trans*-1,4-diaminocyclohexane-*t*CDTA and *trans*-1,4-diaminocyclohexane-*t*CDTA-dimer complexes were in the same range as gadolinium-based contrast agents at 3 Tesla. The $[Fe(\text{en-}t\text{CDTA})]^+$

complex is a pH sensor at weakly acidic pH levels, which are typical for various cancer types.

KEYWORDS

gadolinium, iron chelate, iron oxide nanoparticles, low-molecular-weight iron(III)-based contrast agents, magnetic resonance imaging, nephrogenic systemic fibrosis

1 | INTRODUCTION

The occurrence of nephrogenic systemic fibrosis in patients with disturbed kidney function[1] but especially the deposition of gadolinium originating from linear and macrocyclic gadolinium-based contrast agents (GBCA) in several organs, including, skin, bones, and brain,[2-5] in patients with normal kidney function resulted in the suspension of less stable linear GBCA, with the exception of 2 liver-targeted GBCA (gadoxetic acid and gadobenic acid), by the European Medicines Agency in 2017. Furthermore, there is an ongoing controversy about what has been termed *gadolinium deposition disease*.[6] Although apart from the bones the brain appears to accumulate substantial Gd, it appears not to be the most severely affected organ because even a patient who died of nephrogenic systemic fibrosis had no obvious brain tissue alterations.[4] Thus, other organs and cells, especially of the immune system, should be investigated for evidence of potential gadolinium side effects in the future. This situation, along with the low but increasing contamination of rivers and drinking water by gadolinium,[7-10] has motivated us to investigate low molecular weight iron(III) complexes as iron-based contrast agents (IBCA) for use in MRI, although the more stable macrocyclic GBCA are continued to be considered as safe drugs.

Recently, we have demonstrated that IBCA administered at higher doses than GBCA achieved similar results in typical clinical applications such as dynamic contrast-enhanced MRI and magnetic MRA without the need to modify imaging protocols.[11] Especially the iron(III) complex of *trans*-cyclohexane diamine tetraacetic acid ([Fe(*t*CDTA)]$^-$) provided comparable contrast effects at only twice the typical clinical dose of Magnevist (Bayer AG, Pharmaceuticals, Berlin, Germany, gadolinium diethylenetriaminepentaacetic acid). The relatively strong contrast effect in comparison to [Fe(DTPA)]$^{2-}$ might be attributed to the availability of a water coordination site in [Fe(*t*CDTA)]$^-$.[11,12] Since then, an iron(II) complex of PyC3A, which served as a redox sensor through oxidation of low relaxivity Fe^{2+} to high relaxivity Fe^{3+},[13] and a group of macrocyclic iron complexes with good relaxivities and relatively long persistence in liver and kidneys have been reported.[14,15]

The purpose of this work was to produce several *t*CDTA derivatives by coupling amine-containing compounds to 1 carboxyl group of *t*CDTA and to thus obtain compounds with improved or modified contrast agent properties (Figure 1). The amines we tested were ethylenediamine and *trans*-1,4-diaminocyclohexane to generate *t*CDTA monomers that can serve for chemical coupling purposes and to generate *t*CDTA dimers for reduced rotational times and thus potentially increased relaxivities.[14,16]

2 | METHODS

2.1 | Reagents

If not specified otherwise, all reagents were purchased from Merck KGaA (Darmstadt, Germany).

2.2 | Synthesis of *trans-1,2-diaminocyclohexane-N,N,N′,N′-tetraacetic acid* monoanhydride (*t*CDTA-MA)

6.53 g (17.9 mmol) of *trans*-1,2-diaminocyclohexane-N,N,N′,N′-tetraacetic acid (*t*CDTA) (Carl Roth GmbH, Karlsruhe, Germany) was added to a solution of 12.87 mL (136.2 mmol) acetic anhydride and 2.75 mL pyridine (34.0 mmol). After stirring for 24 h at room temperature under an argon atmosphere, the reaction mixture was filtered and washed with acetic anhydride followed by excess ethyl acetate. The solid was collected and dried under vacuum to give 5.30 g (81.2%) of the white powder *t*CDTA-MA.[17]

2.3 | Synthesis of chelators

2.3.1 | Synthesis of ethylenediamine-*t*CDTA monomer (en-*t*CDTA)

*t*CDTA-MA (14.4 mmol, 5 g) was added in small portions as solid over a period of 6 h to a solution of 19.31 mL ethylenediamine (289 mmol) and 23.75 mL dimethyl sulfoxide under an argon atmosphere. After addition, the reaction mixture was stirred overnight at room temperature. The mixture was then concentrated under reduced pressure (8 mbar) to a thick orange oil that solidified upon standing. The residue was dissolved in methanol and formed a precipitate at room temperature, which was washed several times with methanol to give 3.98 g (80%) of a white solid. Matrix-assisted laser desorption/ionization

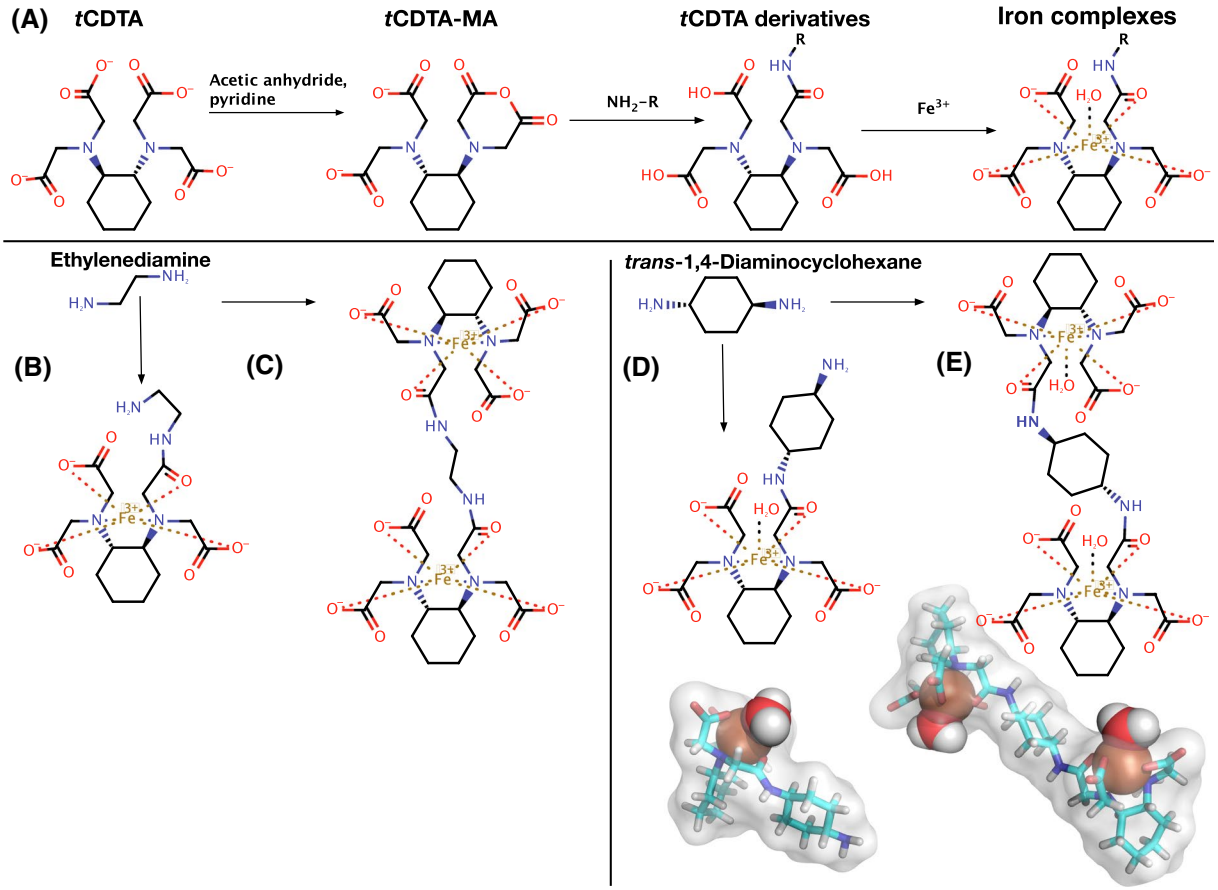

FIGURE 1 Synthesis of *t*CDTA chelator derivatives. (A) First, *t*CDTA-monoanhydride (*t*CDTA-MA) was generated by reaction of *t*CDTA with acetic anhydride and pyridine followed by purification to remove dianhydrides by filtration with acetic anhydride. In the second step, *t*CDTA-MA reacted with amine-containing compounds to give 4 different carboxamide derivatives of *t*CDTA that are shown as chemical structures and corresponding putative molecular models in (B-E). Following the procedure in (A), the reaction of *t*CDTA-MA with ethylenediamine (flexible) in molar excess resulted in the monomer ethylenediamine-*t*CDTA (B), whereas reaction of ethylenediamine with half-molar (or less) ratio to *t*CDTA-MA gave the dimer ethylenediamine-Di-*t*CDTA (C). The reaction of *trans*-1,4-diaminocyclohexane (rigid) in molar excess to *t*CDTA-MA resulted in the monomer *trans*-1,4-diaminocyclohexane-*t*CDTA (D), whereas reaction of *trans*-1,4-diaminocyclohexane in half-molar ratio to *t*CDTA-MA gave the dimer *trans*-1,4-diaminocyclohexane-Di-*t*CDTA (E). *t*CDTA, trans-cyclohexane diamine tetraacetic acid; *t*CDTA-MA, trans-cyclohexane diamine tetraacetic acid–monoanhydride

(MALDI) mass spectrometry measurements (MALDI-TOF/TOF 4700 Proteomics Analyzer, Applied Biosystems, Foster City, USA) gave an expected/measured mass of 389.42/389.18 [M+H]+ (see Supporting Information Figure S2 and S4)—^{1}H-NMR (400 MHz, D_2O): 3.57 (s, 3H), 3.53 (s, 3H), 3.48 (s, 1H), 3.44 (s, 1H), 3.03 (t, 2H), 2.92 (m, 4H), 2.16 (m, 2H), 1.82 (m, 2H), 1.26 (m, 4H); ^{13}C-NMR (D_2O): 170.88, 60.26, 50.86, 39.58, 24.17, 23.29; C,H,N-analysis [%]: C 43.94, H 8.12, N 15.07; calculated for $C_{16}H_{27}N_4O_7(NH_4) \times 2\ H_2O$: C 43.98, H 7.84, N 15.23; maximum deviation: 0.28.

2.3.2 | Synthesis of ethylenediamine-*t*CDTA dimer (en-Di-*t*CDTA)

*t*CDTA-MA (13.5 mmol, 4.66 g) was added in small portions as solid over a period of 6 h to a solution of 0.45 mL ethylenediamine (6.7 mmol), 22.15 mL dimethyl sulfoxide, and 4.36 mL (53.9 mmol) pyridine under argon atmosphere. After addition, the reaction mixture was stirred overnight at room temperature. This mixture was further washed with excess ethanol and then purified by semipreparative high-performance liquid chromatography (HPLC) (5 mM ammonium bicarbonate buffer with pH 7.78, 2% to 66% acetonitrile gradient over 20 min). The fractions containing en-Di-*t*CDTA were identified by HPLC and lyophilized. MALDI mass spectrometry measurements (MALDI-TOF/TOF 4700 Proteomics Analyzer, Applied Biosystems) gave an expected/measured mass of 717.74/699.11 [M+H]+ −18 (dehydration; see Results section and Supporting Information Figure S2 and S4)—1H-NMR (400 MHz, D_2O): 3.65-3.85 (16H), 3.35 (m, 4H), 3.08 (m, 4H), 2.17 (m, 4H), 1.84 (m, 4H), 1.29 (m, 8H)); C,H,N-analysis [%]: C 46.72, H 7.02, N 10.96; calculated for C30H47N6O14Na × 2.15 H2O: C 46.35, H 6.65, N 10.81; maximum deviation: 0.37.

2.3.3 | Synthesis of trans-1,4-diaminocyclohexane-*t*CDTA monomer (trans-*t*CDTA)

*t*CDTA-MA (6.93 mmol, 2.4 g) was added in small portions as solid over a period of 6 h to a solution of 3.17 g *trans*-1,4-diaminoclyclohexane (27.7 mmol) dissolved in 18.24 mL dimethyl sulfoxide under argon atmosphere at approximately 90°C and stirred for another 4 h. The reaction mixture was stirred overnight at room temperature. The mixture was then concentrated under reduced pressure (8 mbar) to an ashen solid. After dissolving in methanol, a precipitate formed at room temperature within 2 days. The precipitate was washed several times with methanol to give 1.89 g (79%) of a white solid. MALDI mass spectrometry measurements (MALDI-TOF/TOF 4700 Proteomics Analyzer, Applied Biosystems) gave an expected/measured mass of 443.51/443.26 [M+H]+ (Supporting Information Figure S2 and S4)—^{1}H-NMR (400 MHz, D_2O): 3.55 (m, 8H), 2.93 (m, 2H), 2.16 (m, 2H), 2.07 (m, 2H), 1.83 (m, 2H), 1.50 (m, 8H), 1.25 (m, 4H); ^{13}C-NMR (D_2O): 172.94, 170.24, 63.16, 60.10, 54.75, 49.08, 48.41, 29.11, 27.98, 24.12, 24.04; C,H,N-analysis [%]: C 51.09, H 8.3, N 13.19; calculated for $C_{20}H_{34}N_4O_7 \times 0.5\ NH_3 \times 1.15\ H_2O$: C 50.92, H 8.08, N 13.36; max. deviation: 0.22).

2.3.4 | Synthesis of trans-1,4-diaminocyclohexane-*t*CDTA dimer (trans-Di-*t*CDTA)

*t*CDTA-MA (17.9 mmol, 5.16 g) was added over 6 h as above to a solution of *trans*-1,4-diaminocyclohexane (7.4 mmol, 0.85 g) in 4.82 mL (59.6 mmol) pyridine and 58.80 mL dimethyl sulfoxide. The reaction mixture was stirred overnight under argon atmosphere at room temperature. The mixture was dried in a rotary evaporator to give a whitish solid. The resulting residue was washed and filtrated with ethanol; the filtrate was collected and then lyophilized to provide a white powder. The MALDI mass spectrometry measurements (Mikroflex MALDI mass spectrometer, Bruker Daltonics, Bremen, Germany) gave an expected/measured mass of 771.83/771.18 [M+H]+ (see Supporting Information Figure S2 and S4)—^{1}H-NMR (400 MHz, D_2O): 3.36 (m, 4H), 3.13 (m, 12H), 2.95 (m, 4H), 2.32 (m, 4H), 1.94 (m, 4H), 1.87 (m, 2H), 1.68 (m, 8H), 1.30 (m, 8H); ^{13}C-NMR (D_2O): 172.68, 60.34, 52.57, 47.73, 38.77, 25.12, 23.47; C,H,N-analysis [%]: C 47.62, H 7.15, N 9.01; calculated for $C_{34}H_{55}N_6O_{14}(HCO_3) \times 3.2\ H_2O$: C 47.21, H 7.06, N 9.44; maximum deviation: 0.43.

2.4 | Synthesis of iron(III) complexes

Iron(III) complexes were prepared by reaction of the *t*CDTA chelators (see above) with a stoichiometric equivalent of $FeCl_3$ solution (1 M, adjusted with a commercial iron chloride calibration solution, final concentrations of 20 to 50 mM) to the binding centers (1:1 ratio for monomers and 2:1 ratio for dimers). Next, the solution was adjusted slowly with a saturated meglumine solution to pH 7.4. After 1 day, the iron complex solutions were centrifuged at 13,800 g for 20 min to remove any excess iron in the form of insoluble iron(III) hydroxide (solubility product 2.8×10^{-39} at 25°C), and the supernatant was filtered with 0.45 µm syringe filters.

2.5 | HPLC analysis

New compounds were assessed after synthesis and purification by reverse-phase HPLC on a Dionex UltiMate 3000 system (Thermo Fisher Scientific, Waltham, USA). The conditions and results are given in the Supplementary Information section Figure S1. Sample detection was performed by absorption measurement at 210 nm using a diode array detector (Dionex UltiMate 3000, Thermo Fisher Scientific, Waltham, USA).

2.6 | Mass spectrometry analysis of chelators

After purification and analysis of the purity by HPLC, the *t*CDTA derivatives were analyzed by MALDI-TOF mass spectrometry in the reflector mode on instruments 4700 Proteomics Analyzer (Applied Biosystems, Foster City, USA) and Microflex LRF (Bruker Daltonics, Bremen, Germany). Measurements were performed by the Shared Facility of Mass Spectrometry of the Institute of Biochemistry, Charité—Universitätsmedizin Berlin. Mass spectrometry results are presented in the Supporting Information Figure S2.

2.7 | Infrared spectroscopy

Infrared spectroscopy spectra of lyophilized substances were recorded on a Bruker Compact FT- infrared spectroscopy spectrometer ALPHA-P using the OPUS software (OPUS 6.5, Bruker Optik GmbH, Germany). See Supporting Information Figure S3.

2.8 | NMR

NMR of the chelators spectra were recorded on a Bruker AV 400 NMR spectrometer (^{1}H and ^{13}C 400 MHz) in D_2O at room temperature. Chemical shifts are reported in ppm relative to residual proton signals of D_2O (4.8 ppm). For NMR spectrometry of trans-Di-*t*CDTA, the sodium salt was used due to the low solubility of the free acid. See also Supporting Information Figure S4.

2.9 | Stability measurement

Stability of the iron complexes (1.0 mM Fe) was compared by measuring the changes in absorption spectra between 220 and 500 nm over time during treatment with 100 mM HCl according to Snyder et al.[14] Additionally, we compared the absorption spectra to those of $FeCl_3$ in 100 mM HCl and *t*CDTA in 100 mM HCl, and $[Fe(tCDTA)]^-$ in 1 M HCl.

2.10 | Cyclic voltammetry

Electrochemical studies were carried out using a EmStat Blue potentiostat (PalmSens BV, Houten, The Netherlands) in a conventional 1-compartment 3-electrode cell with a glassy carbon electrode (ID 1.6 mm) as the working electrode, a platinum plate (5 × 5 mm) as the counter electrode, and a silver wire in aqueous AgCl solution as the pseudo-reference electrode. All measurements were carried out in deionized and degassed H_2O solutions containing 0.1 M KCl at pH 5.9 under argon atmosphere at ambient temperature. Cyclic voltammograms were collected at a scan rate of 0.1 Vs^{-1}. See also Supporting Information Table S1.

2.11 | Relaxivity measurement by relaxometry

For relaxivity measurements, all iron complexes were diluted in water or fetal calf serum (FCS) (Gibco, Thermo Fisher Scientific, Rockford, IL) at concentrations of 0.125, 0.25, 0.5, and 1.0 mM at pH 7.4 and loaded into glass NMR tubes (5 mm outside diameter; Wilmad-Lab Glass, Vineland, USA). Measurements at 0.94 Tesla (T) were performed using an NMR relaxometer Minispec mq 40 (Bruker BioSpin, Rheinstetten, Germany) according to the manufacturer's instructions. For measurements of the pH dependence, samples of $[Fe(en\text{-}tCDTA)]^+$ in the concentrations above were dissolved in water or FCS and adjusted to the different pH values.

2.12 | Relaxivity measurement by MR imaging

Relaxivities at 1.5 T, 3 T, and 7 T were measured on MRI scanners. Up to 7 samples prepared as above were placed in a circular phantom holder at room temperature. For measurements at 37°C, a phantom holder equipped with water heating was kept at 37°C ± 1°C and monitored by a fiber optic temperature probe. Measurements at 1.5 T were conducted on a Magnetom Sonata (Siemens, Erlangen, Germany) and at 3 T on a Magnetom Lumina (Siemens) clinical MRI scanner using standard 2D spin echo sequences. Different repetition times (TR) of 100, 150, 300, 600, and 1000 ms were used to measure T_1 times and calculate T_1 relaxivities. Echo time (TE) was 11 ms for 1.5 T and 13 ms for 3 T. Other imaging parameters were matrix of 256 × 256, field of view (FOV) of 75 × 75 mm^2, and the slice thickness of 5 mm. The T_1 maps were generated from the resulting image datasets using ImageJ with the MRI Analysis Calculator plug-in from Karl Schmidt (v1.0, kfschmidt@bwh.harvard.edu, 2002/06/19).

For measurement at 7 T, the phantoms were imaged on a BioSpec small animal MRI scanner (Bruker, Ettlingen, Germany) using a built-in dedicated multi-TR spin echo sequence with integrated T_1 mapping. The TRs were 25, 72, 125, 186, 258, 346, 459, 617, 882, and 2000 ms. TE was 9.0 ms; an imaging matrix of 256 × 256 was used with a FOV 50 × 50 mm^2 and slice thickness 1 mm.

T_1 times of the samples determined by MRI were measured in circular regions of interest of constant size placed in the center of the cross sections of each tube in the T_1 maps.

The T_1 and T_2 relaxivities were determined by performing linear regression analysis of 1/T versus iron concentration of the complexes using GraphPad Prism version 5.0a (GraphPad Software, Inc., San Diego, CA).

2.13 | Molecular modeling

Molecular modeling of the complexes was done based on the X-ray crystal structures of $[Fe(tCDTA)]^-$[12] using Marvin software followed by Dreiding force field energy minimization (Marvin version 19.17, 2019, ChemAxon, Budapest, Hungary) and the PyMOL Molecular Graphics System (Schrödinger, Inc, New York, USA, Open Source version 1.8.2.1., on Apple XQuartz 2.7.11 X Window System).[18]

3 | RESULTS

In this study, we synthesized *t*CDTA derivatives in 2 steps as shown in Figure 1A using a method adapted from Gestin et al.[17] First, a monoanhydride of *t*CDTA (*t*CDTA-MA) was generated using acetic anhydride in the presence of pyridine as proton acceptor. After separation from dianhydrides by filtration, *t*CDTA-MA was reacted either with an excess of the diamine compounds to generate monomers (defined as the 1:1 condensation reaction product) or with less than half-molar amounts of diamines to synthesize dimers (defined as the 2:1 condensation reaction product). In this way, the reaction with ethylenediamine resulted in the monomer ethylenediamine-*t*CDTA (en-*t*CDTA) (Figure 1B, MW 388.42) and the dimer ethylenediamine-Di-*t*CDTA (en-Di-*t*CDTA) (Figure 1C, MW 716.74). Accordingly, reacting *t*CDTA-MA with an excess of *trans*-1,4-diaminocyclohexane gave the monomer *trans*-1,4-diaminocyclohexane-*t*CDTA (*trans*-*t*CDTA) (Figure 1D, MW 442.51), whereas reaction with a half-molar amount of

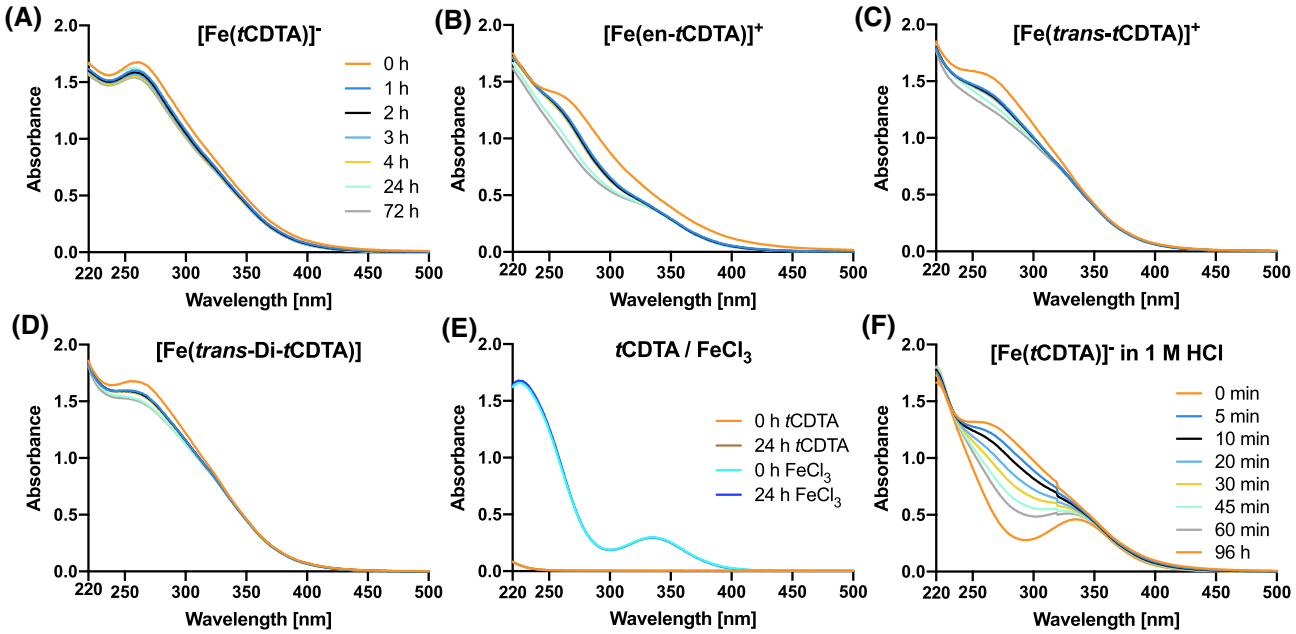

FIGURE 2 Comparison of stabilities of the iron(III) complexes of *t*CDTA and the new derivatives over time. The dissociation of [Fe(*t*CDTA)]$^-$ (A), [Fe(en-*t*CDTA)]$^+$ (B), [Fe(*trans*-*t*CDTA)]$^+$ (C), and [Fe(*trans*-Di-*t*CDTA)] (D) was monitored by measuring absorption spectra (1.0 mM Fe) over time in 100 mM HCl and observing the reduction of absorbance at 300 nm according to Snyder et al.[14] (E) Free $FeCl_3$ has an absorption minimum at 300 nm, and *t*CDTA has only minimal absorption below 250 nm (both in 100 mM HCl). In comparison to harsh treatment with 1 M HCl, which caused a time-dependent dissociation of [Fe(*t*CDTA)]$^-$ (F), all [Fe(*t*CDTA)]$^-$ derivatives were remarkably stable at 100 mM HCl. [Fe(*t*CDTA)]$^-$, iron(III) complex of *trans*-cyclohexane diamine tetraacetic acid; [Fe(en-*t*CDTA)]$^+$, iron(III) complex of ethylenediamine-*t*CDTA; [Fe(trans-*t*CDTA)]$^+$, iron(III) complex of *trans*-1,4-diaminocyclohexane-*t*CDTA; [Fe(*trans*-Di-tCDTA)], iron(III) complex of trans-1,4-diaminocyclohexane-Di-tCDTA

trans-1,4-diaminocyclohexane resulted in the dimer *trans*-1,4-diaminocyclohexane-Di-*t*CDTA (*trans*-Di-*t*CDTA) (Figure 1E, MW 770.83). HPLC analysis (see Supporting Information Figure S1) of purified amides yielded purities with the following peak area percentages—en-*t*CDTA: 98.1%; en-Di-*t*CDTA: 96.6%; *trans*-*t*CDTA: 99.0%; and *trans*-Di-*t*CDTA: 98.4%. Absence of relevant amounts of *t*CDTA was confirmed by HPLC for all chelators, which is an important precondition for relaxivity measurements excluding contributions from the corresponding iron complexes. Product identities were confirmed by MALDI mass spectrometry, ^{1}H and ^{13}C NMR, and elemental analysis (see Supporting Information Figure S4). The main mass peaks of en-Di-*t*CDTA (and to a very small extent, also those of en-*t*CDTA) were reduced by 18 Da, which can be attributed to dehydration during the MALDI mass spectrometry.[19] For confirmation, we compared the infrared spectroscopy spectra of *t*CDTA, *t*CDTA-MA, en-*t*CDTA, and en-Di-*t*CDTA by infrared spectroscopy (see Supporting Information Figure S3). As expected, we found the characteristic bands for anhydrides only for *t*CDTA-MA.

After preparation of the iron(III) complex solutions by letting react the chelators with iron(III) chloride, we compared the stabilities of the new iron complexes with that of [Fe(*t*CDTA)]$^-$, which was reported to have a rather high complex stability constant, log K, of 27.5[20] or of 29.3.[21] Figure 2 (and Supporting Information Figure S5) shows the absorption spectra of the iron(III) complexes over time during a challenge with 100 mM HCl, as done by Snyder et al.[14] All tested complexes revealed only minimal initial absorbance changes at 100 mM HCl and thus differed from iron(III) chloride at 100 mM HCl and to [Fe(*t*CDTA)]$^-$ at 1 M HCl.

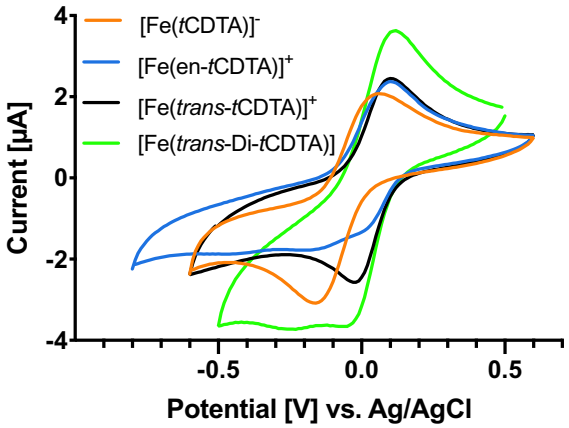

FIGURE 3 Cyclic voltammetry of iron complexes at neutral pH and a scan rate of 100 mV/s. Solutions contained 1.0 mM of the iron complexes and 100 mM KCl as electrolyte

Redox properties of the iron(III) complexes were examined by cyclic voltammetry using a glassy carbon working electrode and KCl as a supporting electrolyte. The peak potential values obtained for the oxidation/reduction events are compiled (referenced to an Ag/AgCl electrode) in Supporting

TABLE 1 T_1 and T_2 relaxivities of iron chelate complexes of *t*CDTA and *t*CDTA derivatives [$mM^{-1}s^{-1}$] per metal ion determined at 0.94, 1.5, 3.0, and 7.0 T (for dimers per molecule in brackets)

Field Strength (temperature)	Solvent	*t*CDTA	Ethylenediamine-*t*CDTA	Ethylenediamine-Di-*t*CDTA	*Trans*1,4-Diaminocyclohexane-*t*CDTA	*Trans*1,4-Diaminocyclohexane-Di-*t*CDTA-Dimer
0.94 T 37°C	r_1 in water	1.56 ± 0.03	0.78 ± 0.01	1.24 ± 0.05 (2.48 ± 0.10)	1.92 ± 0.10	1.99 ± 0.10 (3.98 ± 0.20)
	r_1 in serum	1.99 ± 0.13	0.72 ± 0.02	1.44 ± 0.03 (4.36 ± 0.08)	2.01 ± 0.04	2.18 ± 0.04 (4.36 ± 0.08)
	r_2 in water	1.72 ± 0.06	0.81 ± 0.02	1.50 ± 0.08 (3.00 ± 0.16)	2.16 ± 0.09	2.25 ± 0.29 (4.50 ± 0.58)
	r_2 in serum	2.79 ± 0.36	0.75 ± 0.03	1.68 ± 0.01 (3.36 ± 0.02)	2.49 ± 0.09	2.73 ± 0.03 (5.46 ± 0.06)
1.5 T 23°C	r_1 in water	–	–	–	2.27 ± 0.01	2.75 ± 0.21 (5.50 ± 0.42)
	r_1 in serum	–	–	–	2.74 ± 0.03	3.26 ± 0.41 (6.52 ± 0.82)
3 T 37°C/23°C	r_1 in water	2.07 ± 0.08/2.06 ± 0.13	–	–	2.64 ± 0.04/2.64 ± 0.37	2.99 ± 0.32/2.80 ± 0.03 (5.98 ± 0.64/5.60 ±0.06)
	r_1 in serum	2.35 ± 0.03/2.46 ± 0.17	–	–	3.06 ± 0.07/3.08 ± 0.06	3.39 ± 0.16/3.53 ± 0.02 (6.78 ± 0.32/7.06 ± 0.04)
7 T 37°C/23°C	r_1 in water	1.87 ± 0.04/1.88 ± 0.07	–	–	2.38 ± 0.07/3.40 ± 0.00	2.65 ± 0.15/3.80 ± 0.04 (5.30 ± 0.30/7.60 ± 0.08)
	r_1 in serum	2.71 ± 0.07/2.79 ± 0.04	–	–	2.61 ± 0.26/3.88 ± 0.07	3.23 ± 0.35/4.71 ± 0.37 (6.46 ± 0.70/9.42 ± 0.74)

All measurements were performed in fetal bovine serum or buffer-free water at pH7.4.

r_1, T_1 relaxivity; r_2, T_2 relaxivity; T, Tesla; *t*CDTA, trans-cyclohexane diamine tetraacetic acid.

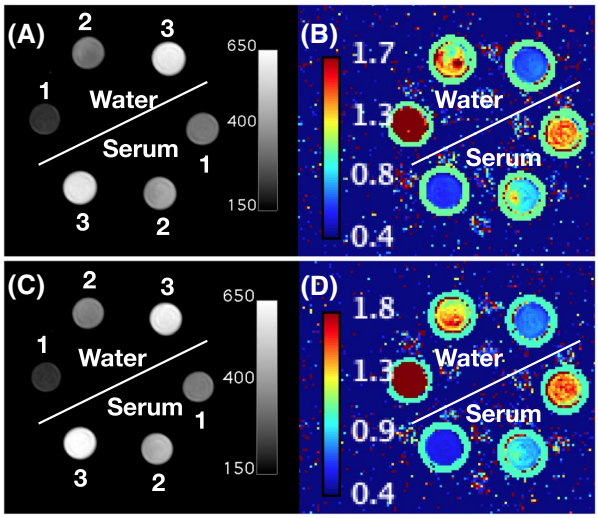

FIGURE 4 Contrast effects of [Fe(*trans*-*t*CDTA)]$^+$ and [Fe(*trans*-Di-*t*CDTA)] in T_1-weighted MR imaging at 3 T. The images show spectrometer tubes containing 3 concentrations (1: 125 μM, 2: 250 μM, and 3: 500 μM Fe) of [Fe(*trans*-*t*CDTA)]$^+$ (A, B) or [Fe(*trans*-Di-*t*CDTA)] (C, D) in water or in 100% fetal bovine serum at neutral pH. (A, C) Signal intensity images acquired with a T_1-weighted spin echo sequence at 3 T (TE 13 ms, TR 150 ms). (B, D) Corresponding T_1 maps in seconds. Images were acquired at 37°C. T, Tesla

Information Table S1. The cyclic voltammograms of all 3 complexes (Figure 3) exhibited 1 reversible redox wave in the anodic scan ($E_a \approx +0.06$ V for [Fe(*t*CDTA)]$^-$ and around +0.1 V for the other complexes). Whereas reversible cathodic waves were observed for [Fe(*t*CDTA)]$^-$ and [Fe(*trans*-*t*CDTA)]$^+$, the other 2 complexes showed 2 small cathodic peak potentials, indicating the presence of 2 different species. Half-wave potentials $E_{1/2}$ in the range of −0.05 to 0.06 V were calculated (Supporting Information Table S1).

Relaxivity, an important measure for the contrast effect, was analyzed at different field strengths (Table 1). The iron complexes of the chelators en-*t*CDTA (Figure 1B) and en-Di-*t*CDTA (Figure 1C), which were generated with ethylenediamine, had relatively low relaxivities at 0.94 T and neutral pH, whereas *trans*-*t*CDTA (Figure 1D) and *trans*-Di-*t*CDTA (Figure 1E) had relaxivities comparable to *t*CDTA at this field strength. However, at higher field strengths the T_1 relaxivities increased substantially and were highest at 7 T for the dimer *trans*-Di-*t*CDTA (Figure 1E), namely 4.71 ± 0.37 $L{\cdot}mmol^{-1}{\cdot}s^{-1}$ per iron and 9.42 ± 0.74 $mM^{-1}s^{-1}$ per dimeric molecule in water and 3.23 ± 0.35 $L{\cdot}mmol^{-1}{\cdot}s^{-1}$/6.46 ± 0.70 $L{\cdot}mmol^{-1}{\cdot}s^{-1}$ in serum (Table 1). Figure 4 demonstrates the contrast effects in MR phantom images of *trans*-*t*CDTA (Figure 4A,B) and *trans*-Di-*t*CDTA (Figure 4C,D) at different concentrations and neutral pH in water and in serum.

The surprisingly low relaxivities of [Fe(en-*t*CDTA)]$^+$ and [Fe(en-Di-*t*CDTA)] compared with [Fe(*trans*-*t*CDTA)]$^+$ and [Fe(*trans*-Di-*t*CDTA)] at neutral pH could be explained by the coordination of the distant amine groups to the chelated iron or alternatively by hydroxide ion coordination (Figure 5). Accordingly, the relaxivities of [Fe(en-*t*CDTA)]$^+$ (Figures 6 and 7) and to a lesser extent of [Fe(en-Di-*t*CDTA)] (Supporting Information Figure S7) determined by relaxometry at 0.94 T increased substantially as the pH was lowered. In water (Figure 6A), en-*t*CDTA had a pH-dependent T_1/T_2 relaxivity increase from 0.82/0.85 $L{\cdot}mmol^{-1}{\cdot}s^{-1}$ at pH 7.4 to 1.77/2.02 $L{\cdot}mmol^{-1}{\cdot}s^{-1}$ at pH 5.1. In serum (Figure 6B), the T_1/T_2-relaxivity increase was threefold, from 0.72/0.75 $L{\cdot}mmol^{-1}{\cdot}s^{-1}$ at pH 7.4 to 2.24/2.73 $L{\cdot}mmol^{-1}{\cdot}s^{-1}$ at pH 5.0. The sigmoidal dose response plots revealed a 50% pH of 6.79 ± 0.07/6.84 ± 0.07 (T_1/T_2) in water and a 50% pH of 6.17 ± 0.11/6.08 ± 0.09 in serum. Figure 6C shows the pH-dependent T_1 relaxivity of [Fe(en-*t*CDTA)]$^+$ at 7 T in serum, which was determined by MR imaging with TR variation on a 7 T Bruker small animal scanner.

The high linearity of the relaxivities of [Fe(en-*t*CDTA)]$^+$ over the measured pH range suggests that they are not a function of [Fe(en-*t*CDTA)]$^+$ concentration and thus of the ratio of [Fe(en-*t*CDTA)]$^+$ to hydroxide ions (see Supporting Information Figure S6). A comparable pH dependence below pH7.4 was observed for the [Fe(en-Di-*t*CDTA)] dimer (see Supporting Information Figure S7B). The relaxivities of the iron complexes coupled with the rigid diamine [Fe(*trans*-*t*CDTA)]$^+$ and [Fe(*trans*-Di-*t*CDTA)] (see Supporting Information Figure S7C,D) were also found to have decreasing relaxivities with increasing pH; however, in contrast to the ethylenediamine derivatives, they exhibited this behavior above pH7.4.

4 | DISCUSSION

Based on the promising results with IBCA, especially with [Fe(*t*CDTA)]$^-$, as potential alternatives that can replace GBCA in contrast-enhanced T_1-weighted MRI,[11] we aimed at modifying *t*CDTA to potentially further improve relaxivities and to generate iron chelates with different molecular properties for various clinical applications.

Using an efficient 2-step synthesis procedure, we created 4 new *t*CDTA derivatives by reaction of 2 different diamine compounds in either an excess or less than half-molar ratio with *t*CDTA-MA, which was generated in the first reaction step. After having confirmed purity of the derivatives and especially the absence of the starting material, *t*CDTA, to rule out a contribution of [Fe(*t*CDTA)]$^-$ to subsequently measured relaxivities and having obtained proof of identity by MALDI mass spectrometry, NMR, and elemental analyses, we made several observations.

The iron complexes of the ethylenediamine derivatives en-*t*CDTA and en-Di-*t*CDTA had surprisingly low T_1 and T_2 relaxivities in comparison to *t*CDTA at neutral pH. It has been shown previously that the substantially lower relaxivity of the 7-coordinated [Fe(DTPA)]$^{2-}$ complex compared

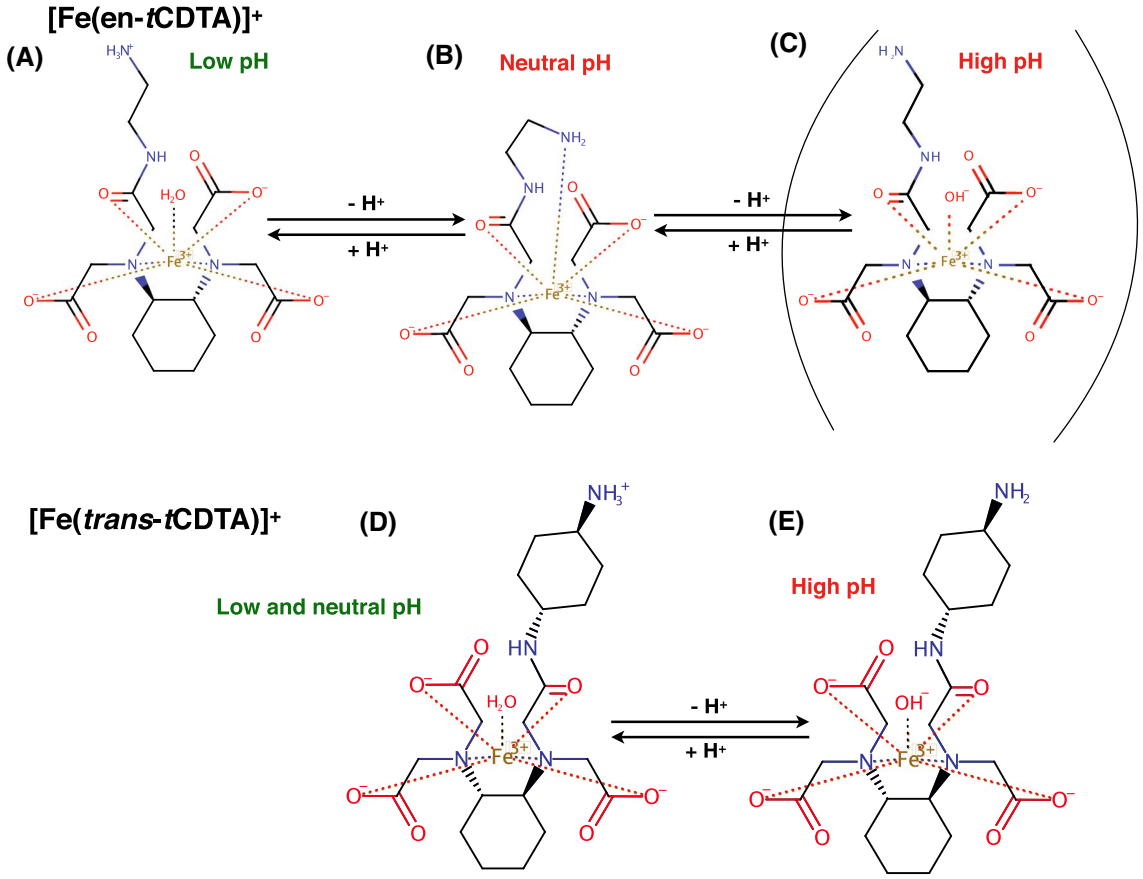

FIGURE 5 Hypothetical mechanisms of the observed pH-dependent relaxivity changes of [Fe(en-*t*CDTA)]$^+$ and [Fe(*trans*-*t*CDTA)]$^+$. (A) At slightly acidic pH, the terminal free amine group could be protonated, which in turn would prevent the iron coordination. Consequently, 1 coordination site would be available for water coordination, allowing efficient inner sphere relaxation. (B) At neutral and high pH, the terminal amine group becomes deprotonated and thus could coordinate to central iron, block water coordination, and prevent efficient inner sphere relaxation. (C) At neutral and higher pH, higher concentrations of hydroxide ions can coordinate the central iron and thus block water coordination and inner sphere relaxation. (B) and (C) could coexist, but (C) seems more likely to occur at higher pHs. (D) The terminal free amine group of the rigid *trans*-1,4-diaminocyclohexane cannot coordinate the iron, which would explain the relatively high relaxivity at neutral and low pH (Supporting Information Figure S7). (E) At higher pH, high concentrations of hydroxide ions can coordinate to iron and thus block water access and reduce relaxivity. The pH-dependent relaxivities of the dimers [Fe(en-Di-*t*CDTA)] and [Fe(*trans*-Di-*t*CDTA)] could be explained accordingly to the correspondent monomers

with the 6-coordinated [Fe(*t*CDTA)]$^-$ complex is due to the fact that in the latter a coordination site remains open for the coordination of water, which allows inner sphere relaxation.[11,12] Analogously, the low relaxivities of [Fe(en-*t*CDTA)]$^+$ and [Fe(en-Di-*t*CDTA)] could be assumed to result from coordination of the terminal amine group in these compounds with the central iron(III), thereby preventing the water coordination and exchange with bulk water, which is required for the important inner-sphere relaxation. This hypothesis (Figure 5) is supported by the strong pH dependence of [Fe(en-*t*CDTA)]$^+$ with a substantial relaxivity increase from neutral pH toward pH 5.0. At low pH, the terminal amine should become protonated, which would prevent coordination of the iron and thus leave 1 Fe coordination site available for water coordination (Figure 5A). Interestingly, the pH levels at which half-maximal T_1 relaxivity occurred were approximately 6.8 in water and 6.2 in serum, which might be explained by electron density reduction of the distal amine group by the amide group of the coupled ethylenediamine, thereby lowering the pKa of the amine. A similar mechanism might explain the relatively low relaxivity and pH dependence of the [Fe(en-Di-*t*CDTA)] dimer, where the 2 introduced amides of the ethylenediamine bridge possibly coordinate with the 2 Fe(III) ions, thereby blocking inner-sphere water coordination and relaxation. Alternatively, the low relaxivities at neutral and higher pHs might be attributable to blockage of the central iron by coordination of hydroxide ions at higher concentrations, which at the same time would prevent inner sphere relaxation (Figure 5C,E). In fact, [Fe(*trans*-*t*CDTA)]$^+$ and [Fe(*trans*-Di-*t*CDTA)] with rigid diamines were also deactivated at higher pHs (Supporting Information Figure S7C,D) but above pH7.4. This pH dependency may be attributed to increased contribution of

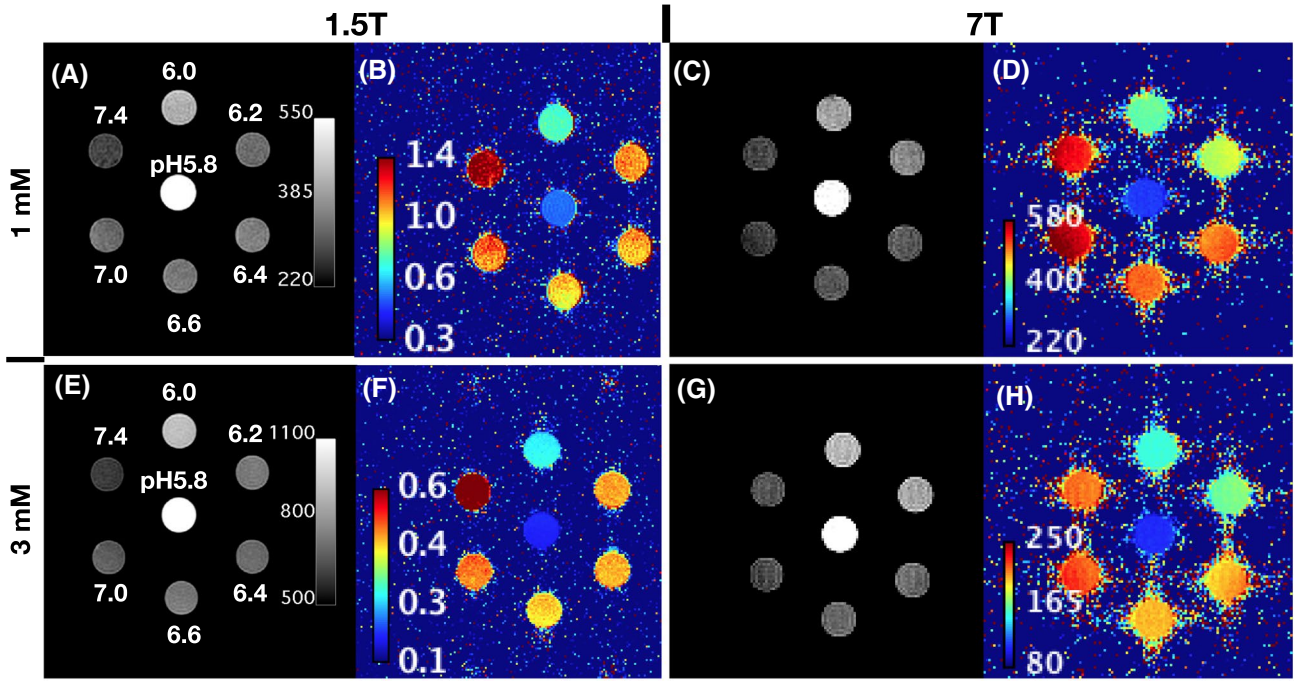

FIGURE 6 MR imaging of pH-dependent contrast effects of $[Fe(en\text{-}t\text{CDTA})]^+$ at 1.5 T and 7 T. Seven spectrometer tubes containing either 1 mM (A-D) or 3 mM (E-F) of $[Fe(en\text{-}t\text{CDTA})]^+$ in 100% fetal bovine serum with adjusted pHs between 5.8 and 7.4 were imaged with a T_1-weighted pulse sequence at magnetic field strengths of 1.5 T and 7 T. (A, E) Signal intensity images (spin echo sequence, TR 150 ms, TE 11 ms) and (B, F) corresponding T_1 maps in seconds acquired in a clinical 1.5 T MRI scanner. (C, G) Signal intensity images (spin echo sequence, TR 71.8 ms, TE 9 ms) and corresponding T_1 maps in milliseconds (D, H) obtained in a Bruker 7 T small animal MRI scanner. Imaging was performed at room temperature

the iron hydroxide complex as pH increases. Furthermore, $[Fe(en\text{-}t\text{CDTA})]^+$ relaxivities were independent of $[Fe(en\text{-}t\text{CDTA})]^+$ concentration and thus the concentration ratio to hydroxide over the full pH range tested (see Supporting Information Figure S6). Therefore, we hypothesize in Figure 5 that the relaxivity decrease of $[Fe(en\text{-}t\text{CDTA})]^+$ with increasing pHs below pH7.4 is dominated by the coordination of the distal amine, whereas for the 2 *trans*-1,4-diaminocyclohexane derivatives, the relaxivity decrease at higher pH is mainly attributable to hydroxide.

Because slightly lower extracellular pH levels are typical for many cancers,[22,23] the pH-dependent T_1 relaxivity increase of $[Fe(en\text{-}t\text{CDTA})]^+$ might be exploited for the detection or characterization of cancer by MRI. Another important example for pH imaging is the identification of salvageable tissue in stroke.[24,25] The low molecular weight complex should be superior to pH nanosensors[26-29] in terms of a faster and broader biodistribution, including a more efficient excretion. The plain activation characteristic and relatively strong T_1 relaxivity increase of $[Fe(en\text{-}t\text{CDTA})]^+$ in comparison to previously reported complex-based T_1-relaxivity pH sensors[30-33] could be advantageous and simplify MR image analysis in the future. Undeniably, clinical use of such pH sensor probes remains challenging because the T_1 contrast effect depends on both relaxivity and local concentration. Nevertheless, probes such as $[Fe(en\text{-}t\text{CDTA})]^+$ can be very useful for preclinical research, for example, when administered by Alzet osmotic pump to achieve constant blood concentrations as demonstrated by Savić et al.[34]

To produce always-on Fe complexes comparable to clinically used GBCA, we chose *trans*-1,4-diaminocyclohexane as a more rigid amine linker molecule that should prevent the potential amine coordination and thus blockage of the important water coordination side. As predicted, the iron complexes of both the monomer *trans*-*t*CDTA and the dimer *trans*-Di-*t*CDTA were shown to have substantially higher relaxivities than their ethylenediamine counterparts at neutral pH (but not at high pH, see above), whereas their relaxivities were not much higher than those of $[Fe(t\text{CDTA})]^-$ at 0.94 T.

Remarkably, T_1 relaxivities of the iron complexes increased with higher magnetic field strengths. $[Fe(trans\text{-}t\text{CDTA})]^+$ and [Fe(*trans*-Di-*t*CDTA)] had especially high relaxivities at the typical clinical field strengths of 1.5 T and 3 T and still high relaxivities at 7 T. This is important, especially considering that the T_1 relaxivities of 2 of the 3 macrocyclic GBCA products currently available clinically in Europe decrease with increasing field strengths.[35] At 3 T, [Fe(*trans*-Di-*t*CDTA)] in blood serum has slightly higher T_1 relaxivity per metal ion than gadoteridol (ProHance, Bracco Diagnostic S.p.S, Milan, Italy) and gadoterate (Dotarem, Guerbet LLC, Paris, France) and slightly lower T_1 relaxivity compared with gadobutrol (Gadovist, Bayer AG, Pharmaceuticals, Berlin, Germany) in blood plasma, whereas

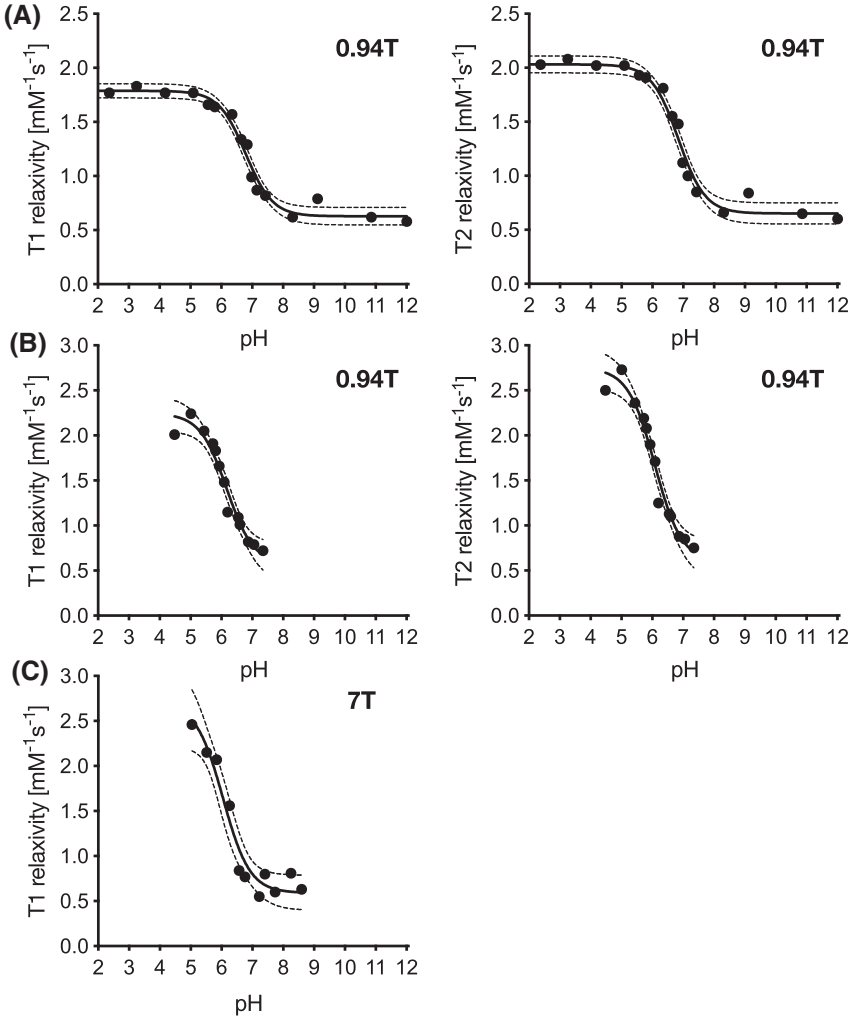

FIGURE 7 $[Fe(en\text{-}t\text{CDTA})]^+$ is a pH sensor. (A) pH dependence of T_1 and T_2 relaxivity of $[Fe(en\text{-}t\text{CDTA})]^+$ in water at 0.94 T. (B) pH dependence of T_1 and T_2 relaxivity of $[Fe(en\text{-}t\text{CDTA})]^+$ in serum at 0.94 T. (B) pH dependence of T_1 and T_2 relaxivities of $[Fe(en\text{-}t\text{CDTA})]^+$ in serum at 7 T. Curves represent the sigmoidal dose-response fits with 95% confidence bands (dotted lines). (A, B) Relaxivities determined with a relaxometer, (C) T_1 values calculated from MR imaging performed in a 7 T Bruker scanner with built-in RARE T_1-mapping sequence

its T_1 relaxivity per molecule is higher than that of all 3 of these products. Field strength-dependent T_1 relaxivity peaked at 7 T for $[Fe(t\text{CDTA})]^-$, whereas it was highest at 3 T for $[Fe(trans\text{-}t\text{CDTA})]^+$ and [Fe(*trans*-Di-*t*CDTA)]. The relaxivity increases in serum in comparison to water were slightly lower than for the mentioned macrocyclic GBCA in plasma, indicating a similar low plasma protein adsorption.[36] Therefore, $[Fe(trans\text{-}t\text{CDTA})]^+$ and [Fe(*trans*-Di-*t*CDTA)] might be potential alternatives to GBCA. Additionally, using the terminal amino group as linker, $[Fe(trans\text{-}t\text{CDTA})]^+$ could serve as an MRI-detectable label, for example, when coupled to specific imaging probes. Because specific probes principally bind to tissue structures, delayed excretion and gadolinium depositions would become even more likely when GBCA would be used for such imaging probes.

Importantly, the very high stability of $[Fe(t\text{CDTA})]^{-20}$ was not substantially reduced by our modifications of *t*CDTA. In fact, like *t*CDTA, all new *t*CDTA derivatives resisted the challenge with 100 mM HCl for 72 h, which was not the case for the macrocyclic iron complexes presented by Snyder et al.[14] We observed a small change in absorption during the first hour, which we attribute to protonation of the chelating amines of *t*CDTA and thus cleavage of the respective coordinative bonds. The rapid time course of this small absorption change for [Fe(*trans*-Di-*t*CDTA)] is shown in Supporting Information Figure S5. However, the iron complexes appeared to retain their stability with the 4 remaining coordinating oxygens. This might also explain, based on the hard and soft acids and bases-principle—hard acid Fe(III) and hard base O—the lower stability of the macrocyclic chelators of Snyder et al., which coordinate with 3 or 4 amines but only with 2 oxygens.[14]

Electrochemical data suggest that the $[Fe(t\text{CDTA})]^-$ complex is not prone to iron redox cycling and thus ROS-induced toxicity under physiological conditions. Merkofer et al. had reported an ascorbyl/monohydroascorbate physiological electrode potential of approx. +0.1 V versus NHE (corresponding to −0.1 V vs. Ag/AgCl,[37] which means that "unproblematic" Fe(III) complexes should show electrode potentials lower than −0.1 V. $[Fe(t\text{CDTA})]^-$ (E_c= −0.16 V vs. Ag/AgCl), which is well below this value, whereas the other complexes are at least close with $E_c \approx 0$ V. However, it should be noted that, for the presented cyclic voltammetry measurements, conditions are not completely matching physiological conditions such as micromolar concentrations of the complexes

and pH 7.[37] It is to be expected that even more negative electrode potentials would result[12] at higher pH values than the value applied here (pH 5.9). The fact that we observed 2 cathodic peak potentials for the [Fe(*trans*-Di-*t*CDTA)] complex and $[Fe(en\text{-}tCDTA)]^+$ might originate from 2 different reasons: the presence of different metal-bound species like Fe-OH_2 and Fe-OH (the aqua form is reduced more readily than the hydroxide form[12]) and/or, in the case of [Fe(*trans*-Di-*t*CDTA)], slightly different potentials for the 2 Fe(III) centers. Future studies will be necessary to thoroughly investigate redox activities under physiological conditions.

Although thermodynamically possible, it is unclear to what degree this redox cycling will occur in blood and other fluids comprising the extracellular spaces. These complexes likely distribute through the extracellular spaces and should be very rapidly and efficiently excreted, suggesting that, even if redox cycling does occur, it is unclear whether transient exposure will lead to any toxic effect.

5 | CONCLUSION

Straightforward 2-step synthesis allowed the generation of 2 derivatives of $[Fe(tCDTA)]^-$, $[Fe(trans\text{-}tCDTA)]^+$ and [Fe(*trans*-Di-*t*CDTA)] with improved relaxivities while preserving high stability compared with $[Fe(tCDTA)]^-$. These new IBCA have favorable relaxivities at 1.5, 3, and 7 T that are in the range of clinically available GBCA. A third derivative, $[Fe(en\text{-}tCDTA)]^+$, provides pH sensing capability and is activated at weakly acidic pH, making it a potential candidate for better MRI-based characterization of cancer tissues or tissue at risk in stroke by MRI.

ACKNOWLEDGMENT

We thank Monika Ebert and Harald Kratz for their practical assistance. We thank Bettina Herwig for language editing. We thank Susanne Müller from the Charité Core Facility 7 T Experimental MRIs for her support. We thank Petra Henklein and Katharina Janek of the Shared Facility of Mass Spectrometry of the Institute of Biochemistry, Charité–Universitätsmedizin Berlin, for performing the MALDI analyses.

ORCID

Eyk Schellenberger https://orcid.org/0000-0003-4096-6865

REFERENCES

1. Grobner T. Gadolinium—a specific trigger for the development of nephrogenic fibrosing dermopathy and nephrogenic systemic fibrosis. *Nephrol Dial Transplant*. 2006;21:1104-1108.
2. Murata N, Gonzalez-Cuyar LF, Murata K, et al. Macrocyclic and other non-group 1 gadolinium contrast agents deposit low levels of gadolinium in brain and bone tissue: preliminary results from 9 patients with normal renal function. *Invest Radiol*. 2016;51:447-453.
3. Gulani V, Calamante F, Shellock FG, et al. Gadolinium deposition in the brain: summary of evidence and recommendations. *Lancet Neurol*. 2017;16:564-570.
4. Fingerhut S, Sperling M, Holling M, et al. Gadolinium-based contrast agents induce gadolinium deposits in cerebral vessel walls, while the neuropil is not affected: an autopsy study. *Acta Neuropathol*. 2018;136:127-138.
5. El-Khatib AH, Radbruch H, Trog S, et al. Gadolinium in human brain sections and colocalization with other elements. *Neurol Neuroimmunol Neuroinflamm*. 2019;6:e515.
6. Layne KA, Wood DM, Dargan PI. Gadolinium-based contrast agents—what is the evidence for 'gadolinium deposition disease' and the use of chelation therapy. *Clin Toxicol (Phila)*. 2020;58:151-160.
7. Lindner U, Lingott J, Richter S, et al. Speciation of gadolinium in surface water samples and plants by hydrophilic interaction chromatography hyphenated with inductively coupled plasma mass spectrometry. *Anal Bioanal Chem*. 2013;405:1865-1873.
8. Birka M, Wehe CA, Hachmöller O, et al. Tracing gadolinium-based contrast agents from surface water to drinking water by means of speciation analysis. *J Chromatogr A*. 2016;1440:105-111.
9. Parant M, Perrat E, Wagner P, et al. Variations of anthropogenic gadolinium in rivers close to waste water treatment plant discharges. *Environ Sci Pollut Res Int*. 2018;25:36207-36222.
10. González V, Vignati DAL, Pons M-N, et al. Lanthanide ecotoxicity: first attempt to measure environmental risk for aquatic organisms. *Environ Pollut*. 2015;199:139-147.
11. Boehm-Sturm P, Haeckel A, Hauptmann R, et al. Low-molecular-weight iron chelates may be an alternative to gadolinium-based contrast agents for T1-weighted contrast-enhanced MR imaging. *Radiology*. 2018;286:537-546.
12. Seibig S, van Eldik R. Structural information on trans-1, 2-diaminocyclohexane-N, N -tetraacetateferrate (III) in the solid and aqueous phase. *Inorg Chim Acta*. 1998;279:37-43.
13. Wang H, Jordan VC, Ramsay IA, et al. Molecular magnetic resonance imaging using a redox-active iron complex. *J Am Chem Soc*. 2019;141:5916-5925.
14. Snyder EM, Asik D, Abozeid SM, et al. A new class of Fe(III) macrocyclic complexes with alcohol donor groups as effective T1 MRI contrast agents. *Angew Chem Int Ed*. 2020;59:2414-2419.
15. Asik D, Smolinski R, Abozeid SM, et al. Modulating the properties of Fe(III) macrocyclic MRI contrast agents by appending sulfonate or hydroxyl groups. *Molecules*. 2020;25:2291.
16. Caravan P, Farrar CT, Frullano L, et al. Influence of molecular parameters and increasing magnetic field strength on relaxivity of gadolinium- and manganese-based T1 contrast agents. *Contrast Media Mol Imaging*. 2009;4:89-100.
17. Gestin JF, Faivre-chauvet A, Mease RC, et al. Introduction of five potentially metabolizable linking groups between 111In-cyclohexyl EDTA derivatives and F(ab')2 fragments of anti-carcinoembryonic antigen antibody–I. A new reproducible synthetic method. *Nucl Med Biol*. 1993;20:755-762.
18. DeLano WL. *The PyMOL Molecular Graphics System*. San Carlos, CA: DeLano Scientific; 2002.
19. Giordanengo R, Viel S, Allard-Breton B, et al. Tandem mass spectrometry of poly(methacrylic acid) oligomers produced by negative mode electrospray ionization. *J Am Soc Mass Spectrom*. 2009;20:25-33.

20. Fornasiero D, Bellen JC, Baker RJ, et al. Paramagnetic complexes of manganese(II), iron(III), and gadolinium(III) as contrast agents for magnetic resonance imaging. The influence of stability constants on the biodistribution of radioactive aminopolycarboxylate complexes. *Invest Radiol*. 1987;22:322-327.
21. Bond J, Jones TI. Iron chelates of polyaminocarboxylic acids. *Trans Faraday Soc*. 1959;55:1310-1318.
22. Webb BA, Chimenti M, Jacobson MP, et al. Dysregulated pH: a perfect storm for cancer progression. *Nat Rev Cancer*. 2011;11:671-677.
23. Thews O, Riemann A. Tumor pH and metastasis: a malignant process beyond hypoxia. *Cancer Metastasis Rev*. 2019;38:113-129.
24. Wu L, Jiang L, Sun PZ. Investigating the origin of pH-sensitive magnetization transfer ratio asymmetry MRI contrast during the acute stroke: correction of T_1 change reveals the dominant amide proton transfer MRI signal. *Magn Reson Med*. 2020;84:2702-2712.
25. Harston GWJ, Tee YK, Blockley N, et al. Identifying the ischaemic penumbra using pH-weighted magnetic resonance imaging. *Brain*. 2015;138:36-42.
26. Lu J, Sun J, Li F, et al. Highly sensitive diagnosis of small hepatocellular carcinoma using pH-responsive iron oxide nanocluster assemblies. *J Am Chem Soc*. 2018;140:10071-10074.
27. Caro C, García-Martín ML, Pernia Leal M. Manganese-based nanogels as pH switches for magnetic resonance imaging. *Biomacromol*. 2017;18:1617-1623.
28. Li B, Gu Z, Kurniawan N, et al. Manganese-based layered double hydroxide nanoparticles as a T_1 -MRI contrast agent with ultrasensitive pH response and high relaxivity. *Adv Mater*. 2017;29.
29. Yang L-M, Zheng H, Ratnakar JS, et al. Engineering a pH-sensitive liposomal MRI agent by modification of a bacterial channel. *Small*. 2018;14:e1704256.
30. Zhang S, Wu K, Sherry AD. A novel pH-sensitive MRI contrast agent. *Angew Chem Int Ed Engl*. 1999;38:3192-3194.
31. Moriggi L, Yaseen MA, Helm L, et al. Serum albumin targeted, pH-dependent magnetic resonance relaxation agents. *Chemistry*. 2012;18:3675-3686.
32. Raghunand N, Howison C, Sherry AD, et al. Renal and systemic pH imaging by contrast-enhanced MRI. *Magn Reson Med*. 2003;49:249-257.
33. Garcia-Martin ML, Martinez GV, Raghunand N, et al. High resolution pH(e) imaging of rat glioma using pH-dependent relaxivity. *Magn Reson Med*. 2006;55:309-315.
34. Savić T, Gambino G, Bokharaie VS, et al. Early detection and monitoring of cerebral ischemia using calcium-responsive MRI probes. *Proc Natl Acad Sci USA*. 2019;116:20666-20671.
35. Szomolanyi P, Rohrer M, Frenzel T, et al. Comparison of the relaxivities of macrocyclic gadolinium-based contrast agents in human plasma at 1.5, 3, and 7 T, and blood at 3 T. *Invest Radiol*. 2019;54:559-564.
36. Rohrer M, Bauer H, Mintorovitch J, et al. Comparison of magnetic properties of MRI contrast media solutions at different magnetic field strengths. *Invest Radiol*. 2005;40:715-724.
37. Merkofer M, Kissner R, Hider RC, et al. Fenton chemistry and iron chelation under physiologically relevant conditions: electrochemistry and kinetics. *Chem Res Toxicol*. 2006;19:1263-1269.

SUPPORTING INFORMATION

Additional Supporting Information may be found online in the Supporting Information section.

FIGURE S1 HPLC
FIGURE S2 MALDI Mass spectrometry
FIGURE S3 Infrared spectroscopy
FIGURE S4 Nuclear magnetic resonance analysis
FIGURE S5 Absorbance change of [Fe(trans-Di-*t*CDTA)] in 100 mM HCl during first hour. (A) Corresponding to figure 2, a small change of the absorption spectrum of [Fe(trans-Di-*t*CDTA)] was recorded during first hour (interval 2 min) after diluting in 100 mM HCl. (B) Time-course of absorption at 300 nm. The rapid change (exponential decay, $K = 0.130 \pm 0.007$) during the first minutes might be explained by protonation of the chelating amines and thus cleavage of the respective coordinative bonds (but maintaining stability through coordinative oxygen bonds, Figure 2)
FIGURE S6 Relaxivity determination of Fe[en-*t*CDTA]$^+$ calculated from relaxometer measurements at 0.94T. x-axis: Fe[en-*t*CDTA]$^+$ concentrations [mM] iron; y-axis: 1/T1 in [1/s]
FIGURE S7 Comparison of the pH-dependent relaxivities of the iron(III)-*t*CDTA derivates coupled with flexible ethylenediamine (*en*) versus rigid trans-1,4-diaminocyclohexane (*trans*). (A) [Fe(en-*t*CDTA)]$^+$ monomer, (B) [Fe(en-Di-*t*CDTA)] dimer, (C) [Fe(*trans*-*t*CDTA)]$^+$ monomer, and (D) [Fe(*trans*-Di-*t*CDTA)] dimer. The relaxivity decrease occurred for the en derivates below pH7.4 and for the trans derivatives above pH 7.4. Relaxivities were measured on a relaxometer at 0.94T and 37°C in water
TABLE S1 Cyclic voltammetry. Cathodic, anodic and half-wave potentials of iron-complexes

How to cite this article: Xie J, Haeckel A, Hauptmann R, et al. Iron(III)-*t*CDTA derivatives as MRI contrast agents: Increased T_1 relaxivities at higher magnetic field strength and pH sensing. *Magn Reson Med*. 2021;85:3370–3382. https://doi.org/10.1002/mrm.28664